Author Gate

Journal of Medicine and Health Studies

Shaqra University

Original Article

Computational Approaches for Lead Discovery against SARS-CoV-2 3C-Like Protease: Virtual Screening and Molecular Dynamics Studies

Mohammad Khan[1], Feras Almarshad[2]

[1]Department of Bioengineering, Integral University, Lucknow, Uttar Pradesh, India.

[2]Department of Internal Medicine, College of Medicine, Shaqra University, Shaqra, Saudi Arabia.

CORRESPONDING AUTHOR

Mohammad Kalim Ahmad Khan
Department of Bioengineering, Integral University, Lucknow-226026, UP, India.
Email: mkakhan@iul.ac.in

https://orcid.org/0000-0002-8004-1448

Received: 13 Nov 2023
Accepted: 27 Nov 2023
Published: 30 Dec 2023

DOI
10.37881/jmahs.225

ABSTRACT

Background: The COVID-19 pandemic has caused significant difficulties in multiple emotional, social, and financial areas. Despite the positive effects of vaccination in reducing infection and fatality rates, the need for efficient antiviral medications, particularly those that can be taken orally, remains a critical concern.
Methods: A virtual screening method based on structure, referred to as SBVS, was used to identify potential inhibitory small molecules that specifically target the 3C-like protease ($3CL^{PRO}$) found in SARS-CoV-2.
Results: The filtering process for potential ligands involved strict criteria based on their molecular properties, including a molecular weight limit of 500 g/mol, maximum of five hydrogen bond donors, maximum of 10 hydrogen bond acceptors, and logP limit of 5. This was done to identify five candidates with lower ΔG values than the reference drugs lopinavir (-8.19 kcal/mol) and ritonavir (-8.04 kcal/mol). Three hits were identified through further evaluation using the hydrogen bond criteria and the BOILED-Egg model. The pharmacokinetic attributes of these two hits were compared with those of the reference drugs lopinavir and ritonavir.
Conclusion: The molecular dynamics simulation (20 ns) outcomes unequivocally demonstrated the stability and promising nature of MCULE-2367618737 as a possible lead compound against the targeted $3CL^{PRO}$.
Keywords: SBVS, Docking, ADMET, SARS-CoV-2, $3CL^{PRO}$, Molecular dynamics.

INTRODUCTION

SARS-CoV-2, also referred to as the 2019 novel coronavirus (2019-nCoV), is a highly contagious member of the human coronavirus (HCoV) family that has caused widespread and severe COVID-19. It is classified under the β category of coronaviruses (CoVs) and belongs to one of four genera, including α, β, γ, and δ, with the first two affecting mammals and the latter two affecting birds. Respiratory Syndrome Coronaviruses (SARS-CoV, MERS-CoV, and SARS-CoV) have caused respiratory infections in various regions.[1-3] As of November 8, 2023, the WHO has reported 771,820,937 cases and 6,978,175 deaths globally. To combat the persistent pandemic, standard preventive measures such as wearing face masks, practicing hand hygiene, maintaining social distance, implementing lockdowns, and working remotely have been widely adopted. However, predicting the behavior of a virus owing to its adaptive mutations remains a challenging task for scientists. To address this issue, the scientific community has identified potential oral drug molecules that may hinder viral replication. The SARS-CoV-2 genome encodes 3C-

like protease ($3CL^{PRO}$), sometimes referred to as the main protease (M^{PRO}) or nonstructural protein 5 (NSP5), which is an important therapeutic target and is required during viral replication for the catalysis of polyproteins into non-structural proteins (NSPs).[4]

$3CL^{PRO}$ is a 306-amino acid polypeptide consisting of three domains, each spanning a different number of amino acids. The first domain contains 8-101 amino acids, the second contains 102-184 amino acids, and the third contains 201-303 amino acids. The tertiary structure of the protein folds into five alpha helices that are distributed across a large, antiparallel globular structure. This globular structure is connected to the second domain through a 185-200 residue-long loop. The catalytic dyad includes a cysteine residue located at the 145^{th} position in the second domain along with a histidine located at position 41 in the first domain.[5,6] Proton transfer from cysteine 145 to histidine 41 occurs during the acylation and diacylation phases of the activation process. Because $3CL^{PRO}$ is essential to both transcription and viral replication, it is a prime target for therapeutic intervention against SARS-CoV-2. The purpose of this work was to find novel small-molecule inhibitors that target the residues in the substrate-binding crevices.[7-10] The study used structure-based virtual screening (SBVS) with search parameters including lipophilicity (logP < 5), hydrogen bond acceptor (HBA ≤ 10), hydrogen bond donor (HBD ≤ 5), and molecular weight (MW ≤ 500 Da) in order to do this. The comprehensive digital investigational ligand archive of MCULE was used for the screening, and AutoDock Vina (ADV), which is integrated with the MCULE drug discovery platform, was used for docking with $3CL^{PRO}$.[11,12]

Based on physicochemical parameters such as topological surface area (TPSA) and WLOGP, toxicity evaluations, and the Brain or Intestinal EstimateD (BOILED)-Egg model were used to evaluate the potential for human intestinal absorption (HIA) and blood-brain barrier (BBB) penetration. The research assessed the drug-like characteristics of the chosen compounds in addition to Pfizer's research into the Brenk alert, PAINS, and Lipinski rule of five. Molecular dynamics (MD) simulations were used to evaluate ligand hit stability. To ascertain the experimental lead's potential for inhibition, a comparison between the lead molecule and the reference medication, lopinavir, was conducted.[13,14] This multidisciplinary strategy combines several scientific methods to improve our comprehension of possible countermeasures for SARS-CoV-2. The results of this investigation offer important new information for the creation of COVID-19 treatments.

MATERIALS AND METHODS

3D structure retrieval and energy minimization of protein

We obtained a 2.16 Å resolution three-dimensional crystal structure of SARS-CoV-2 $3CL^{PRO}$ (6LU7) from the RCSB PDB database.[9] We eliminated all other elements—heteroatoms, ions, and extra molecules—to leave only the protein's apo-form in order to provide an appropriate three-dimensional input file for the chosen molecular interaction programme.

To optimize the conformation and structural integrity of the target protein, we conducted an energy minimization process using SwissPDB viewer. This step involved refining the protein structure to minimize unfavorable interactions and stabilize the molecule, thereby ensuring a more accurate representation of the protein's native state for subsequent computational analyses.[15-18]

Structural-based virtual screening for targeted drug discovery

We used the online MCULE drug discovery platform, for target-based screening. This platform harbours over five million ligands that can be synthesized on order, and then purchased. Our search was limited by Pfizer's rule of five (RO5), which limits the molecular weight (MW) to ≤ 500 Da, the hydrogen bond

donors must not be more than 5 (HBD ≤ 5), a restricted number of hydrogen bond acceptors (HBA ≤ 10), and a partition coefficient (LogP) of ≤ 5 to filter small molecules.[19]

To ensure a diverse range of compounds, we set the sample size to 1000. Additionally, we implemented a resemblance search threshold of 0.90 for the input query. We used the FP2 fingerprint in Open Babel as a 2D search method to carry out the SBVS procedure. By keeping the remaining search parameters at their default settings, we aimed to exhaustively examine the potential ligands that satisfied the specified criteria.[20]

Obtaining 3D Structures of Reference Drugs Lopinavir and Ritonavir

The SDF files for lopinavir's (CID: 92727) and ritonavir's (CID: 392622) 2D structures were acquired from the National Centre for Biotechnology Information's PubChem database.[20-22] Utilizing Accelrys Discovery Studio Visualizer (DSV), conversion from the two-dimensional representation to their respective three-dimensional structures was carried out with high accuracy. This involved translating the chemical structures into their three-dimensional conformations. Energy minimization was performed using the same protocol for the receptor molecule to ensure the structural integrity and optimize the conformation of the inhibitors. This step aimed to refine and stabilize the 3D structures of lopinavir and ritonavir by aligning their conformations for further computational analyses and modeling.[14,21,22]

Utilizing AutoDock Vina for molecular docking

The MCULE online drug discovery platform, which incorporates AutoDock Vina, facilitates molecular docking simulations between $3CL^{PRO}$ and ligands sourced from SBVS. To begin these simulations, a 3D structure of the protein in PDB format was submitted to AutoDock Vina port on the MCULE platform. To ensure the reliability of docking results, a grid size was set to encompass the specific binding pocket of the protein.[23,24]

Docking parameters were left at their default values, including exhaustiveness and the number of binding variants per ligand. The free energy of binding (ΔG) was used to determine the best binding position of ligand candidates within the $3CL^{PRO}$ binding site. In order to provide information about possible binding affinities and orientations, this measure is essential in determining and prioritising the best interactions between the ligands and the protein's binding crevice.[25,26]

Evaluating potentially harmful moieties in screened ligands

An investigation was undertaken using the toxicity checker integrated within the MCULE resource portal to identify toxic moieties, fragments, and substructures within the ligand hits. This assessment used a stringent and comprehensive SMARTS algorithm to detect and flag any chemical components within the virtually screened ligands that could pose risks to human health or the environment.[19]

Assessing absorption and permeation using the BOILED-Egg model

The anticipated ligands were tested for potential human intestinal absorption (HIA) and blood-brain barrier (BBB) penetration using the SwissADME tool's BOILED-Egg model, also referred to as the Egan Egg model. This model utilizes two key physicochemical features: WLOGP (with a reference value of ≤ 5.88) for assessing lipophilicity and TPSA (with a reference value of ≤ 131.6 $Å^2$) for evaluating apparent polarity. The BOILED-Egg model provides a visual representation of the deviation of a molecule from the optimal characteristics required for favorable absorption. This pictorial aid facilitates an understanding of a molecule's proximity to the desired attributes for potential absorption into the human

body, thereby aiding in the estimation of its likelihood for effective uptake and permeation across the blood-brain barrier.[27–30]

Evaluating medicinal chemistry characteristics

As part of the assessment of medicinal chemistry features, promiscuous compounds—also referred to as frequent hitters—were identified by means of the SwissADME tools' Pan Assay Interference Structure (PAINS) alert option. This procedure uses the Ruth Brenk alert to identify harmful moieties, dyes, and unwanted substructures. This helps identify components of compounds that could interfere with assays or have characteristics that are considered unsuitable for medicinal chemistry applications.[31,32]

Assessing stability via molecular dynamics simulation

Utilising GROMACS 5.1.2 at a molecular mechanics level (MM) of 300K, a series of computational simulations were carried out to assess the stability of the optimal ligand-$3CL^{PRO}$ complex and the reference medication, lopinavir-$3CL^{PRO}$. Using the gmx grep programme, the ligands were separated from the associated complexes. The force field characteristics and structural configuration of the selected ligand hits were predicted using the CGenFF (CHARMm general force field) service.[33-35] Additionally, $3CL^{PRO}$ topologies were generated using the pdb2gmx modules of GROMACS 5.1.2. Every complex was put inside a dodecahedron-shaped box with a 10-Å margin of separation, filled with water molecules. The steepest descent algorithm was then applied to them in a 250,000-step reduction phase. The system temperature was then raised via the equilibration phase from 0 K to 300 K in 10 nanoseconds while maintaining constant NVT and NPT conditions. After equilibration, a particle mesh was created using the Ewald technique. Several GROMACS modules, including rms, rmsf, sasa, ΔGsolv, Rg, and HB, were used to analyse the compounds' mobility and stability in order to look into the molecular dynamics.[36–38] The following parameters provided valuable information regarding RMSD, SASA, Rg, and HB graphs of the complexes, thereby facilitating a comprehensive assessment of their stability.

RESULTS

Structure-based virtual screening analysis

Utilizing the strict criteria set by Pfizer's Lipinski RO5, we extensively screened a vast library of investigational ligands from the MCULE digital repository.[19] Out of the initial 52,321,324 hits, 28,323,823 ligand hits exhibited substantial docking within the $3CL^{PRO}$ binding pocket. Through a comprehensive evaluation process, we prioritized the top 100 molecules based on their binding free energy.

After a rigorous toxicity assessment, 25 molecules were identified as potential candidates. As shown in Figure 1, these SBVS hits were further refined based on the binding free energy (ΔG) and hydrogen bond formations. After the screening procedure, two ligands with ΔG values of -8.19 kcal/mol and -8.04 kcal/mol, respectively, were found. These values were lower than or comparable to those of the control medications, lopinavir and ritonavir.[11,39]

Docking simulation and toxicity assessment of ligand hits

Using the MCULE ADV tool to perform a docking analysis of $3CL^{PRO}$, the binding affinities of all virtually screened ligands and reference inhibitors, lopinavir and ritonavir, were assessed. The computed binding free energy (ΔG) of the ligand hits varied between -9.33 kcal/mol and -8.78 kcal/mol.

A comparative analysis was performed between the docked complexes of the predicted ligands and $3CL^{PRO}$ against the reference drugs lopinavir and ritonavir. Lopinavir displayed a ΔG value of -8.19 kcal/mol upon docking into the binding pocket of $3CL^{PRO}$, engaging with 15 residues through four types

of binding mechanisms, namely hydrogen bonding (HB), Van der Waals (Vdw), Pi-Cation, and alkyl interactions (Figure 2).

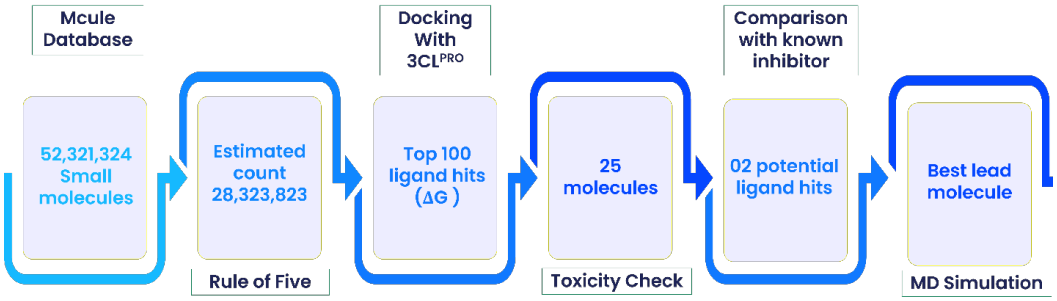

Figure 1: Flowchart outlining the SBVS methodology employed in identifying the most promising lead molecule targeting the 3CL^{PRO} of SARS-CoV-2.

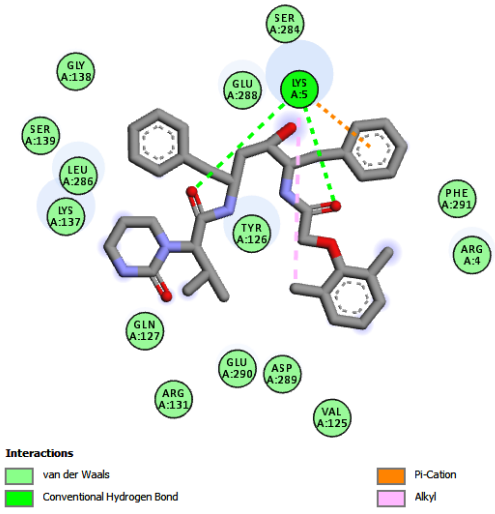

Figure 2: 2D representation of the molecular interaction between lopinavir (control) and 3CL^{PRO}, showcasing engagement through Vdw, two hydrogen bonds (HB), Alkyl, and Pi-Cation forces during protein-ligand docking.

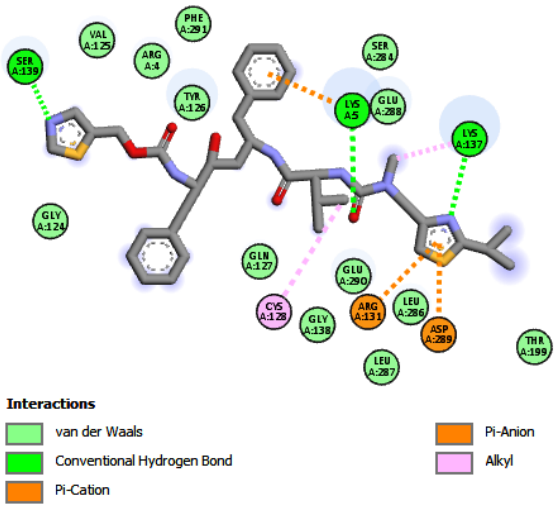

Figure 3: 2D representation of the molecular interaction between ritonavir (control) and 3CL^{PRO}, showcasing engagement through Vdw, three hydrogen bonds, Pi-Alkyl, Pi-Anion, and Pi-Carbon forces during protein-ligand docking.

Contrarily, when ritonavir was docked into the binding pocket of $3CL^{PRO}$, it showed a ΔG value of -8.04 kcal/mol. It interacted with 19 residues via five distinct binding interactions, including hydrogen bonding (HB), Van der Waals (Vdw), Pi-Alkyl, Pi-Anion, and Pi-Carbon interactions. (Figure 3).
After conducting the toxicity assessment, only 25 ligands emerged as potential drug candidates. Among these, we proceeded solely with the hits exhibiting ΔG values equal to or lesser than the control drugs. This stringent criterion led to identifying five molecules, as detailed in Table 1.

Table 1: Molecular interactions and binding affinity of the top five hit compounds and positive control with $3CL^{PRO}$.

Ligands	$3CL^{PRO}$	
	ΔG ($kcalmol^{-1}$)	Types of molecular interactions
MCULE-2367618737	-9.33	Vdw, HB (3), CHB, Pi-Pi T-Shaped, and Pi-Alkyl
MCULE-2221338441	-8.78	Vdw, HB (3), CHB, Pi-Alkyl, Alkyl, Pi-Sigma, and Halogen (Fluorine)
MCULE-6231272498	-8.83	Vdw, HB (1), CHB, Pi-Pi T-Shaped, Alkyl, and Pi-Alkyl
MCULE-6906097724	-8.81	Vdw, HB (1), CHB, Pi-Alkyl, Pi-Anion, Pi-Carbon, and Pi-Pi Stacked
MCULE-1620403711	-9.18	Vdw, HB (3), CHB, Pi-Alkyl, and Halogen (Fluorine)
Lopinavir	-8.19	Vdw, HB (2), Alkyl, and Pi-Cation
Ritonavir	-8.04	Vdw, HB (3), Pi-Alkyl, Pi-Anion, and Pi-Carbon

Vdw: Van der Waals, HB: Conventional Hydrogen Bond, CHB: Carbon Hydrogen Bond

Assessment of Human Intestinal Absorption and Blood-Brain Barrier permeation via BOILED-Egg filtration

As its designation suggests, the model differentiates between yellow and white regions, indicating their predictive positions for significant Blood-Brain Barrier (BBB) penetration and Human Intestinal Absorption (HIA) permeation. Among the three ligand hits, MCULE-2367618737, MCULE-2221338441, and MCULE-1620403711 demonstrated three hydrogen bonds comparable to the potential control molecule lopinavir. Consequently, these three hits and both control molecules were evaluated by BOILED-Egg filtration.
MCULE-1620403711 and MCULE-2367618737 among them showed reasonable HIA permeation. MCULE-2009284974 was the only chemical that showed no signs of HIA permeability or BBB penetration. While the positive control drug and the ligand hits did not show BBB penetration, the reference drug lopinavir did show significant HIA permeability. Furthermore, ritonavir did not fall into the BBB or HIA prediction range of the model.
The BOILED-Egg prediction for the reference and ligand molecules is shown in Figure 4, where P-gp-negative and P-gp-positive molecules are denoted by red and blue dots, respectively. This distinction indicates that ligands that are P-glycoprotein substrates are ejected after BBB penetration, while ligands that are not substrates may pass through the brain barrier.

Drug-likeness beyond Lipinski's Rule of Five

Small molecules hoping to become promising oral lead compounds had their drug-likeness evaluated qualitatively using the Ghose, Veber, Egan, and Muegge criteria. Among these ligands, MCULE-2367618737 did not comply with Ghose's two parameters. MCULE-2221338441 exhibited violations in the Ghose, Veber, Egan, and Muegge rules, whereas MCULE-1620403711 adhered to all the discussed criteria. The first control drug, lopinavir, displayed violations in the Ghose, Veber, and Muegge rules,

and the second control drug, ritonavir, exhibited violations in the Ghose, Veber, Egan, and Muegge criteria. However, all ligands and control molecules presented an Abbott BS value of 0.55, indicating significant oral absorption characteristics, except for ritonavir (0.17), as presented in Table 2.

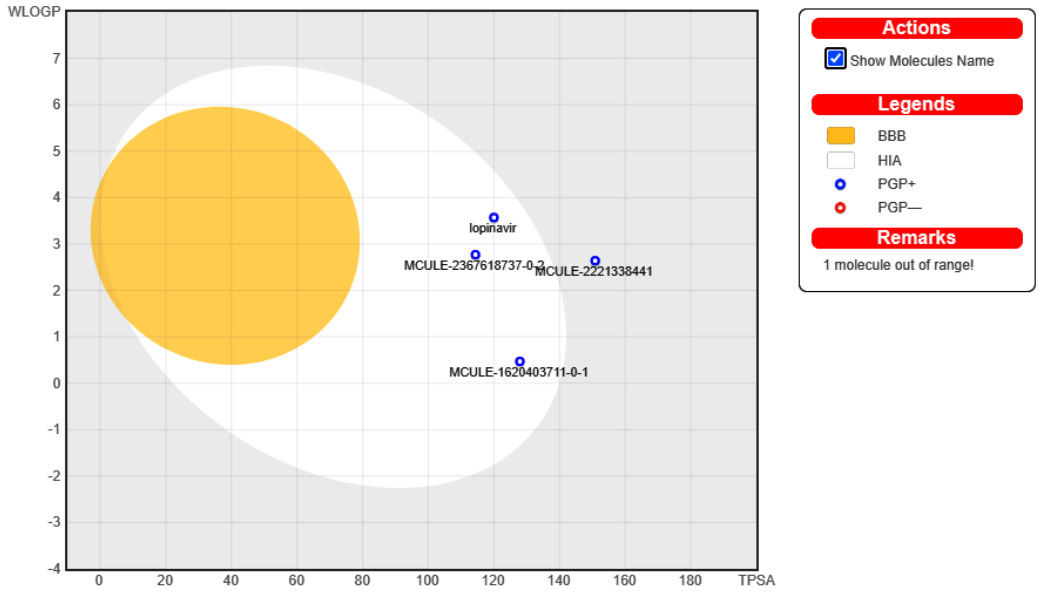

Figure 4: The BOILED-Egg model assesses passive HIA permeation and BBB penetration of ligands alongside control molecules lopinavir and ritonavir. MCULE-2367618737 and MCULE-1620403711, located in the egg white region, indicate HIA permeation, while MCULE-2009284974 shows comparatively less HIA absorption. The reference drug, lopinavir, demonstrates substantial HIA permeation, but neither the ligand hits nor the positive control drug exhibits BBB permeation. Additionally, ritonavir falls outside the model's predicted HIA or BBB penetration range.

Table 2: Predicted drug-likeness beyond Lipinski's Rule of Five for ligands and control drugs.

Molecule	Ghose	Veber	Egan	Muegge	Abbott BS
	Violation(s)				
MCULE-2367618737	2	0	0	0	0.55
MCULE-2221338441	2	1	1	1	0.55
MCULE-1620403711	0	0	0	0	0.55
Lopinavir (Control)	3	1	0	3	0.55
Ritonavir (Control)	4	2	1	4	0.17

Medicinal chemistry attribute assessment

The results of the assessment of medicinal chemistry attributes for the ligands and control drugs were as follows: none of the ligands and control molecules displayed any alerts for PAINS, except for one Brenk alert for MCULE-2221338441 and MCULE-1620403711. All molecules, including the reference drugs, were found to have violations of lead-likeness, as presented in Table 3. Furthermore, the data on synthetic accessibility indicated that the ligands were relatively easier to synthesize than control drugs.

Table 3, which offers a thorough examination of the medicinal chemistry characteristics of the ligands and control medications, including their lead-likeness, synthetic accessibility values, and PAINS and Brenk warnings, summarises the aforementioned findings.

Table 3: Medicinal chemistry attributes analysis for ligands and control drugs

Molecule	PAINS alert	Brenk alert	Lead-likeness	Synthetic accessibility
MCULE-2367618737	0	0	1	3.65
MCULE-2221338441	0	1	1	4.86
MCULE-1620403711	0	1	2	4.39
Lopinavir (Control)	0	0	3	5.67
Ritonavir (Control)	0	0	3	6.45

Hydrogen bond analysis during molecular interactions

During the binding interactions with the target protein $3CL^{PRO}$, the reference drug ritonavir demonstrated the presence of three conventional hydrogen bonds. Similarly, three ligand hits, MCULE-2367618737, MCULE-2221338441, and MCULE-1620403711, exhibited three hydrogen bonds comparable to the control molecule ritonavir. Notably, these ligands displayed robust binding affinities with more negative ΔG values upon docking with the target protein residues.

The compounds with the highest number of hydrogen bonds and the strongest binding affinity, when compared to the control molecules, were chosen for additional examination. MCULE-2221338441 was excluded from consideration because of its low HIA permeation, according to the BOILED-egg model. However, MCULE-2367618737 and MCULE-1620403711 displayed three hydrogen bonds in their molecular interactions with $3CL^{PRO}$. As illustrated in Figure 5, MCULE-2367618737 connected with 16 residues through five different binding interactions: hydrogen bonds (HB), Van der Waals (Vdw), carbon-hydrogen bonds (CHB), Pi-Pi T-Shaped, and Pi-Alkyl interactions. Its ΔG value was -9.33 kcal/mol. Similar to this, Figure 6 shows that MCULE-1620403711 interacted with 15 residues through five different binding interactions: Vdw, three hydrogen bonds, CHB, Pi-Alkyl, and Halogen (Fluorine) interactions. It also revealed a ΔG value of -9.18 kcal/mol.

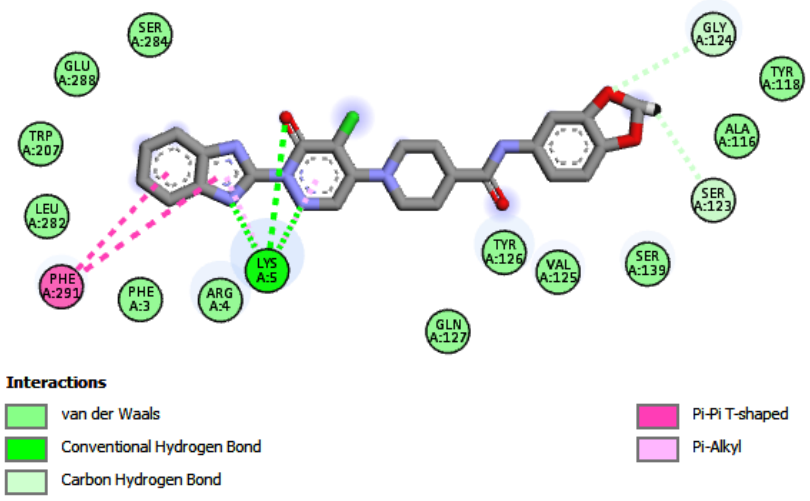

Figure 5: 2D representation of the molecular interaction between MCULE-2367618737 and $3CL^{PRO}$, showcasing engagement through Vdw, 3HBs, CHB, Pi-Pi T-Shaped, and Pi-Alkyl forces during protein-ligand docking.

Assessing the stability of docked complexes via MD Simulation

In order to evaluate the stability of the complexes of the reference drug lopinavir and the top two ligand hits (MCULE-2367618737 and MCULE-1620403711), we ran molecular dynamics simulations for 20 ns

using the GROMACS software. To examine the stability of molecular interactions within the ligands and protein-docked complexes, we plotted graphs representing RMSD, SASA, Rg, and HBs.[16,40,41]

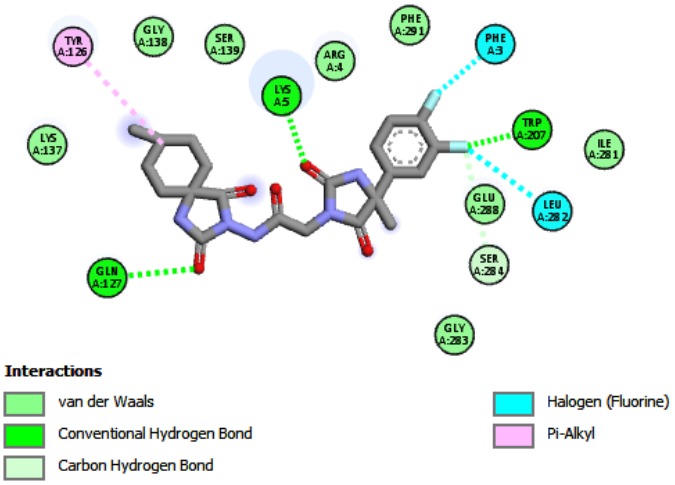

Figure 6: 2D representation of the molecular interaction between MCULE-1620403711 and 3CL^{PRO}, showcasing engagement through Vdw, 3HBs, CHB, Pi-Alkyl, and Halogen (Fluorine) forces during protein-ligand docking.

Root-mean-square deviation (RMSD) analysis

Using RMSD as a measure, the stability of the docked complexes was examined. The reference inhibitor lopinavir (black), the expected ligand hits MCULE-2367618737 (red), and MCULE-1620403711 (green) were found to have mean relative standard deviations of 0.27 nm, 0.19 nm, and 0.21 nm, respectively, when complexed with 3CL^{PRO}. The reference molecule lopinavir and other ligands with 3CL^{PRO} produce a complex that is less stable than the one generated by 3CL^{PRO} and MCULE-2367618737, according to the RMSD plot (Figure 7).

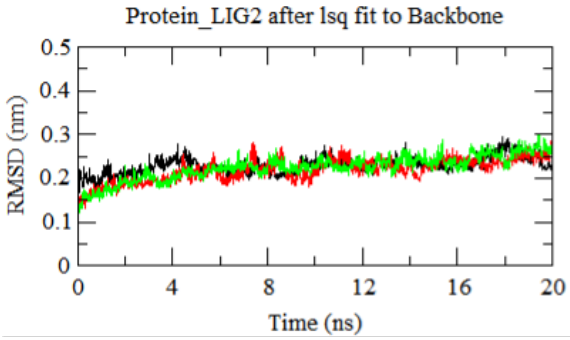

Figure 7: Time-dependent RMSD Plot. Black, red, and green denote values calculated for 3CL^{PRO}-lopinavir, MCULE-2367618737, and MCULE-1620403711, respectively.

Solvent-accessible surface area (SASA) analysis

Figure 8 depicts the surface area of the protein exposed to the solvent molecules using the SASA plot. Following the binding of lopinavir (black), MCULE-2367618737 (red), and MCULE-1620403711 (green), the average SASA values associated with 3CL^{PRO} were 16.22 nm^2, 15.64 nm^2, and 15.89 nm^2, respectively.

Radius of gyration (Rg) analysis

Rg shows an inverse connection with compactness and is used as an indication of how compact docked complexes are. For the docked complexes of lopinavir, MCULE-2367618737, and MCULE-1620403711, the

average Rg values with $3CL^{PRO}$ were found to be 2.21 nm, 2.12 nm, and 1.98 nm, in that order (as depicted in Figure 9).

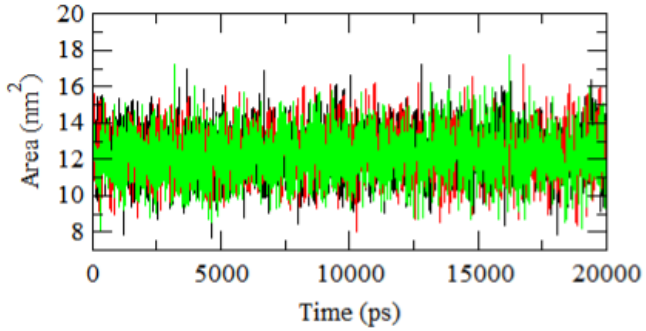

Figure 8: Time-dependent SASA Plot. Black, red, and green denote values calculated for $3CL^{PRO}$-lopinavir, MCULE-2367618737, and MCULE-1620403711, respectively.

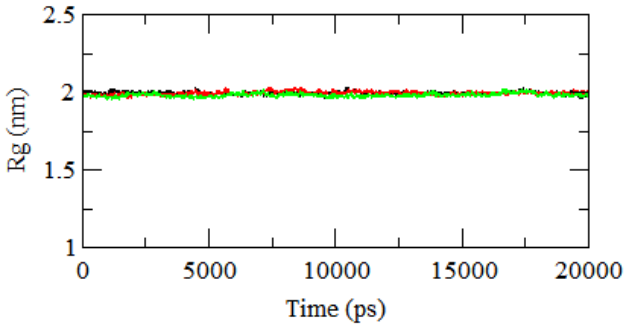

Figure 9: Time-dependent Rg Plot. Black, red, and green denote values calculated for $3CL^{PRO}$-lopinavir, MCULE-2367618737, and MCULE-1620403711, respectively.

Hydrogen bond analysis during MD simulation

The hydrogen bond (HB) plot in Figure 10 illustrates the HB formation count, deformations, and stability throughout the molecular dynamics (MD) simulations. This plot shows the docked complex involving the reference drug, lopinavir, and protein $3CL^{PRO}$. Furthermore, the nature of HB creation and deformation during the 20 ns MD simulations for MCULE-2367618737 and MCULE-1620403711, respectively, is depicted in Figures 11 and 12.

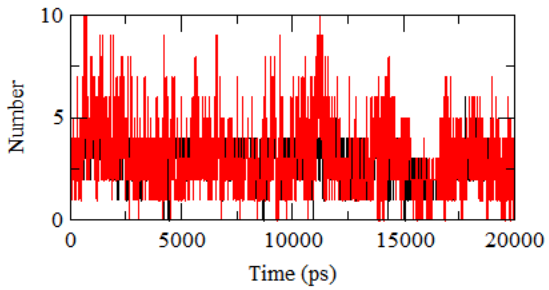

Figure 10: HB Plot for $3CL^{PRO}$-lopinavir (control drug) complex

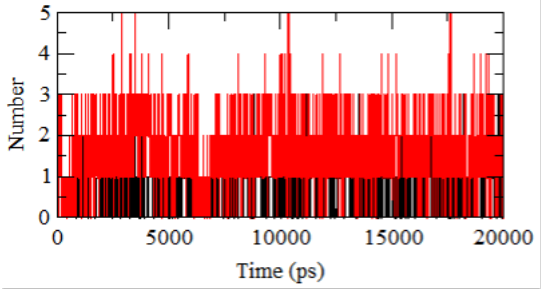

Figure 11: HB Plot for $3CL^{PRO}$- MCULE-2367618737 complex

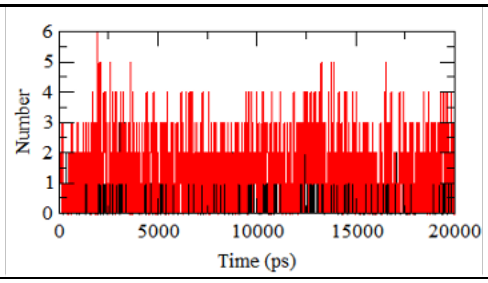

Figure 12: HB Plot for 3CL^{PRO}- MCULE-1620403711 complex

DISCUSSION

The Lipinski's Rule of Five criterion from Pfizer was used in this study's stringent screening procedure to find possible therapeutic candidates that target the 3CL^{PRO} of SARS-CoV-2. From over 52 million initial hits, 25 promising ligands emerged, and after further scrutiny based on the binding free energy and hydrogen bond formation, five molecules stood out. These findings were crucial in narrowing the selection to two lead ligands with remarkable binding affinities comparable to those of the control drugs, lopinavir, and ritonavir.

Docking simulations and toxicity assessments revealed essential insights into how these ligands interact with the 3CL^{PRO} binding pocket. The structural interactions, illustrated in Figures 2 and 3, showcased the bonding modes and residues engaged by lopinavir and ritonavir, providing a basis for comparison with potential drug candidates.

Subsequent evaluation via the BOILED-Egg filtration model sheds light on the potential of ligands for Human Intestinal Absorption (HIA) and Blood-Brain Barrier (BBB) penetration. Although the ligand hits, including the control drugs, exhibited substantial HIA permeation, none penetrated the BBB, essential for targeting viral infections in the central nervous system.

They assessed drug-likeness beyond Lipinski's Rule of Five, highlighting discrepancies in adherence to various parameters. Despite some violations, the molecules, including lead candidates, displayed significant oral absorption characteristics, indicating their potential as oral lead compounds.

Medicinal chemistry attribute assessments suggested promising features with minimal alerts for problematic molecular structures (PAINS), although they showed lead-likeness violations. However, their synthetic accessibility is comparatively favorable, providing a practical advantage for their potential development.

Analysis of hydrogen bonding during molecular interactions emphasized the presence of three hydrogen bonds in the lead candidates, a trait shared with ritonavir. These bonds and robust binding affinities make the lead candidates MCULE-2367618737 and MCULE-1620403711 stand out, reinforcing their potential as effective drug candidates.

Additional stability evaluation using Molecular Dynamics (MD) simulations gave important information about the complexes that the reference medication lopinavir and the top two ligand hits generated. The lead ligand, MCULE-2367618737, demonstrated exceptional stability in the docking complex with 3CL^{PRO}, suggesting a more robust interaction than the reference molecule.

All these results highlight the potential of lead ligands as prospective therapeutic options against SARS-CoV-2, especially MCULE-2367618737 and MCULE-1620403711. Despite limitations in BBB penetration, their strong binding affinities, favorable oral absorption characteristics, and stability in interactions with the target protein make them compelling candidates for further development and optimization of potential drugs for COVID-19 treatment.

CONCLUSION

Two promising lead candidates, MCULE-2367618737 and MCULE-1620403711, have emerged from a thorough examination of compounds targeting the $3CL^{PRO}$ of SARS-CoV-2. These candidates showed notable binding affinities and robust molecular interactions similar to those of the approved control medications, lopinavir and ritonavir. However, they cannot cross the blood-brain barrier, limiting their potential for targeting viral infections in the central nervous system. Despite this limitation, these lead compounds possess favorable medicinal chemistry attributes, synthetic accessibility, and stability in complex formation with $3CL^{PRO}$, as determined by Molecular Dynamics (MD) simulations. These attributes make them promising drug candidates for further development and optimization. These lead compounds offer promising drug development prospects against SARS-CoV-2, given their significant binding affinities and adherence to critical drug development criteria. Further studies and optimization processes can build on these foundational elements to develop effective therapeutics to combat COVID-19.

Acknowledgments

The authors express their gratitude to the Deanship of Scientific Research at the University of Hail, Saudi Arabia for their financial and technical support through project number COVID-1916.

Financial support and sponsorship

Deanship of Scientific Research, University of Hail, Saudi Arabia, project number COVID-1916.

Conflict of Interest

The authors declare that there is no conflict of interest relevant to this article.

REFERENCES

1. Tiwari U, Bano A, Khan MKA. A review on the COVID-19: Facts and current situation. *NeuroPharmac J.* 2021; 6(02):180-191.
2. Khan MKA, Pokharkar NB, Al-Khodairy FM, Al-Marshad FM, Arif JM. Structural Perspective on Molecular Interaction of IgG and IgA with Spike and Envelope Proteins of SARS-CoV-2 and Its Implications to Non-Specific Immunity. *Biointerface Res Appl Chem*. 2020;11(3):10923–39.
3. Kin N, Miszczak F, Lin W, Gouilh MA, Vabret A; EPICOREM Consortium. Genomic Analysis of 15 Human Coronaviruses OC43 (HCoV-OC43s) Circulating in France from 2001 to 2013 Reveals a High Intra-Specific Diversity with New Recombinant Genotypes. *Viruses*. 2015 May 7;7(5):2358-77.
4. Muramatsu T, Takemoto C, Kim YT, Wang H, Nishii W, Terada T, Shirouzu M, Yokoyama S. SARS-CoV 3CL protease cleaves its C-terminal autoprocessing site by novel subsite cooperativity. *Proc Natl Acad Sci U S A*. 2016 Nov 15;113(46):12997-13002.
5. Liu X, Wang XJ. Potential inhibitors against 2019-nCoV coronavirus M protease from clinically approved medicines. *J Genet Genomics*. 2020 Feb 20;47(2):119-121.
6. Iketani S, Forouhar F, Liu H, Hong SJ, Lin FY, Nair MS, Zask A, Huang Y, Xing L, Stockwell BR, Chavez A, Ho DD. Lead compounds for the development of SARS-CoV-2 3CL protease inhibitors. *Nat Commun*. 2021;12(1):2016.
7. Jin Z, Du X, Xu Y, Deng Y, Liu M, Zhao Y, Zhang B, et al. Structure of M^{pro} from SARS-CoV-2 and discovery of its inhibitors. *Nature*. 2020 Jun;582(7811):289-293.
8. Świderek K, Moliner V. Revealing the molecular mechanisms of proteolysis of SARS-CoV-2 M^{pro} by QM/MM computational methods. *Chem Sci*. 2020 Jun 25;11(39):10626-10630.

9. Jin Z, Du X, Xu Y, Deng Y, Liu M, Zhao Y, et al. The crystal structure of COVID-19 main protease in complex with an inhibitor N3. *Nature*;2020;582(7811):289–93.
10. Mishra A, Waghela R. A Comparative Study of Approved Drugs for SARS-CoV-2 by Molecular Docking. *Journal of Molecular Docking*. 2021;1(1):25–31.
11. Khan MKA, Alouffi S, Ahmad S. Identifying potential inhibitors of C-X-C motif chemokine ligand10 against vitiligo: structure-based virtual screening, molecular dynamics simulation, and principal component analysis. *J Biomol Struct Dyn*. 2023;11:1-18.
12. Khan MKA, Ahmad S, Rabbani G, Shahab U, Khan MS. Target-based virtual screening, computational multiscoring docking and molecular dynamics simulation of small molecules as promising drug candidate affecting kinesin-like protein KIFC1. *Cell Biochem Funct*. 2022;40(5):451-472.
13. Hariyanto TI, Kristine E, Jillian Hardi C, Kurniawan A. Efficacy of Lopinavir/Ritonavir Compared With Standard Care for Treatment of Coronavirus Disease 2019 (COVID-19): A Systematic Review. *Infect Disord Drug Targets*. 2021;21(5):e270421187364.
14. Narayanan N, Nair DT. Ritonavir may inhibit exoribonuclease activity of nsp14 from the SARS-CoV-2 virus and potentiate the activity of chain terminating drugs. *Int J Biol Macromol*. 2021;168:272-278.
15. Morris GM, Goodsell DS, Halliday RS, Huey R, Hart WE, Belew RK, et al. Automated docking using a Lamarckian genetic algorithm and an empirical binding free energy function. *J Comput Chem*. 1998;19(14):1639–62.
16. Khan FI, Lai D, Anwer R, Azim I, Khan MKA. Identifying novel sphingosine kinase 1 inhibitors as therapeutics against breast cancer. *J Enzyme Inhib Med Chem*. 2020;35(1):172-186.
17. Ahmad KMK, Salman A, Al-Khodairy Salman F, Al-Marshad Feras M, Alshahrani Abdulrahman M, Arif Jamal M. Computational Exploration of Dibenzo [a,l] Pyrene Interaction to DNA and its Bases: Possible Implications to Human Health. *Biointerface Res Appl Chem*. 2020;11(4):11272–83.
18. Brooks BR, Bruccoleri RE, Olafson BD, States DJ, Swaminathan S, Karplus MC: A program for macromolecular energy, minimization, and dynamics calculations. *J Comput Chem*. 1983;4(2):187–217.
19. Kiss R, Sandor M, Szalai FA. http://Mcule.com: a public web service for drug discovery. J Cheminform. 2012 Dec 1;4(S1):P17.
20. Shakil S. Molecular interaction of investigational ligands with human brain acetylcholinesterase. *J Cell Biochem*. 2019 Jul;120(7):11820-11830.
21. Macchiagodena M, Pagliai M, Procacci P. Characterization of the non-covalent interaction between the PF-07321332 inhibitor and the SARS-CoV-2 main protease. *J Mol Graph Model*. 2022;110:108042.
22. Dayer MR, Taleb-Gassabi S, Dayer MS. Lopinavir; A Potent Drug against Coronavirus Infection: Insight from Molecular Docking Study. *Arch Clin Infect Dis*. 2017;12(4).
23. Trott O, Olson AJ. AutoDock Vina: improving the speed and accuracy of docking with a new scoring function, efficient optimization, and multithreading. *J Comput Chem*. 2010 Jan 30;31(2):455-61.
24. Ajijur R, Salman A, Ahmad KMK. Combinatorial Design to Decipher Novel Lead Molecule against Mycobacterium tuberculosis. *Biointerface Res Appl Chem*. 2021;11(5):12993–3004.
25. Khan MKA, Akhtar S, Arif JM. Development of In Silico Protocols to Predict Structural Insights into the Metabolic Activation Pathways of Xenobiotics. *Interdiscip Sci*. 2018;10(2):329-345.
26. Khan MKA, Akhtar S, Arif JM. Structural Insight into the Mechanism of Dibenzo[a,l]pyrene and Benzo[a]pyrene-Mediated Cell Proliferation Using Molecular Docking Simulations. *Interdiscip Sci*. 2018;10(4):653–73.
27. Daina A, Michielin O, Zoete V. SwissADME: a free web tool to evaluate pharmacokinetics, drug-likeness and medicinal chemistry friendliness of small molecules. *Sci Rep*. 2017;7:42717.
28. Attique SA, Hassan M, Usman M, Atif RM, Mahboob S, Al-Ghanim KA, Bilal M, Nawaz MZ. A Molecular Docking Approach to Evaluate the Pharmacological Properties of Natural and Synthetic Treatment Candidates for Use against Hypertension. *Int J Environ Res Public Health*. 2019;16(6):923.

29. Egan WJ, Merz KM Jr, Baldwin JJ. Prediction of drug absorption using multivariate statistics. *J Med Chem*. 2000;43(21):3867-77.
30. Egan WJ, Lauri G. Prediction of intestinal permeability. *Adv Drug Deliv Rev*. 2002;54(3):273-89.
31. Baell JB, Holloway GA. New substructure filters for removal of pan assay interference compounds (PAINS) from screening libraries and for their exclusion in bioassays. *J Med Chem*. 2010;53(7):2719-40.
32. Brenk R, Schipani A, James D, Krasowski A, Gilbert IH, Frearson J, Wyatt PG. Lessons learnt from assembling screening libraries for drug discovery for neglected diseases. *ChemMedChem*. 2008;3(3):435-44.
33. Van Der Spoel D, Lindahl E, Hess B, Groenhof G, Mark AE, Berendsen HJ. GROMACS: fast, flexible, and free. *J Comput Chem*. 2005;26(16):1701-18.
34. Vanommeslaeghe K, MacKerell AD Jr. Automation of the CHARMM General Force Field (CGenFF) I: bond perception and atom typing. *J Chem Inf Model*. 2012;52(12):3144-3154.
35. Vanommeslaeghe K, Hatcher E, Acharya C, et al. CHARMM general force field: A force field for drug-like molecules compatible with the CHARMM all-atom additive biological force fields. *J Comput Chem*. 2010;31(4):671-690.
36. Petersen HG. Accuracy and efficiency of the particle mesh Ewald method. J Chem Phys. 1995;103(9):3668–79.
37. Stenberg S, Stenqvist B. An Exact Ewald Summation Method in Theory and Practice. *J Phys Chem A*. 2020;124(19):3943-3946.
38. Fischer NM, van Maaren PJ, Ditz JC, Yildirim A, van der Spoel D. Properties of Organic Liquids when Simulated with Long-Range Lennard-Jones Interactions. *J Chem Theory Comput*. 2015;11(7):2938-2944.
39. Ahmad Khan MK, Akhtar S, Al-Khodairy F. Molecular docking approach to elucidate metabolic detoxification pathway of polycyclic aromatic hydrocarbons. NeuroPharmac Journal. 2021;6:150–61.
40. Ali S, Khan FI, Mohammad T, Lan D, Hassan MI, Wang Y. Identification and Evaluation of Inhibitors of Lipase from *Malassezia restricta* using Virtual High-Throughput Screening and Molecular Dynamics Studies. *Int J Mol Sci*. 2019;20(4):884.
41. Kuzmanic A, Zagrovic B. Determination of ensemble-average pairwise root mean-square deviation from experimental B-factors. *Biophys J*. 2010;98(5):861-871.